



1 **Expansion of oil palm and other cash crops causes an increase of land surface temperature**
2 **in Indonesia**

3

4 Clifton R. Sabajo^{1,2†}, Gueric le Maire³, Tania June⁴, Ana Mejjide¹, Olivier Roupsard^{3,5},

5 Alexander Knohl^{1,6}

6

7 ¹ University of Goettingen, Bioclimatology, 37077 Göttingen, Germany

8 ² AgroParisTech – Centre de Montpellier, Agropolis International, 648 rue Jean-François

9 Breton, 34093 Montpellier, France

10 ³ CIRAD, UMR Eco&Sols, F-34398 Montpellier, France

11 ⁴ Agrometeorology Laboratory Department of Geophysics and Meteorology,

12 Faculty of Mathematics and Natural Sciences, Bogor Agricultural University (IPB), Indonesia

13 ⁵ CATIE (Centro Agronómico Tropical de Investigación y Enseñanza / Tropical Agriculture

14 Centre for Research and Higher Education), 7170 Turrialba, Costa Rica

15 ⁶ University of Goettingen, Centre of Biodiversity and Sustainable Land Use (CBL), 37073

16 Goettingen, Germany

17

18 † Correspondence: Clifton R. Sabajo, University of Goettingen, Bioclimatology, Büsungenweg 2,

19 37077 Göttingen, Germany. E-mail: csabajo@uni-goettingen.de

20 Telephone: +49 (0) 551 39 12114

21

22

23 **Abstract**

24

25 Indonesia is currently one of the regions with the highest transformation rate of the land surface

26 worldwide due to the expansion of oil palm plantations and other cash crops replacing forests

27 on large scales. Land cover changes, which modify land surface properties, have a direct effect



28 on the land surface temperature (LST), a key driver for many ecological functions. Despite the
29 large historic land transformation in Indonesia toward oil palm and other cash crops and
30 governmental plans for future expansion, this is the first study so far to quantify the impact of
31 land transformation in Indonesia on LST. We analyse LST from the thermal band of a Landsat
32 image and produce a high resolution surface temperature map (30m) for the lowlands of the
33 Jambi province on Sumatra (Indonesia), a region of large land transformation towards oil palm
34 and other cash crops over the past decades. We compare LST, albedo, Normalized Differenced
35 Vegetation Index (NDVI), and evapotranspiration (ET) of seven different land cover types
36 (forest, urban areas, clear cut land, young and mature oil palm plantations, acacia and rubber
37 plantations) and show that forests have lower surface temperatures than these land cover types
38 indicating a local warming effect after forest conversion with LST differences up to 10.09 ± 2.6
39 °C (mean \pm SD) between forest and clear cut land. The differences in surface temperatures are
40 explained by an evaporative cooling effect offsetting an albedo warming effect. Our analysis of
41 the LST trend of the past 16 years based on MODIS data shows that the average daytime surface
42 temperature of the Jambi province increased by 1.05 °C, which followed the trend of observed
43 land cover changes and exceed the effects of climate warming. Our study provides evidence
44 that the expansion of oil palm plantations and other cash crops leads to changes in biophysical
45 variables, warming the land surface and thus enhancing the increase in air temperature due to
46 climate change.

47

48

49 *Keywords:* Land surface temperature, albedo, NDVI, evapotranspiration, biophysical variables,
50 oil palm, remote sensing, Landsat, MODIS, Indonesia, land-use / land cover change

51

52



53 **1 Introduction**

54

55 Indonesia is one of the regions where the expansion of cash crop monocultures such as acacia
56 (timber plantation), rubber, oil palm plantations and smallholder agriculture has drastically
57 reduced the area of primary forest in the past decades (Bridhikitti and Overcamp, 2012;
58 Drescher et al., 2016; Marlier et al., 2015; Miettinen et al., 2012; Verstraeten et al., 2005). This
59 large scale conversion of rainforest for agricultural use has been observed on the island of
60 Sumatra, which has experienced the highest primary rainforest cover loss in all of Indonesia
61 (Drescher et al., 2016; Margono et al., 2012; Miettinen et al., 2011). Forest cover in the
62 Sumatran provinces of Riau, North Sumatra and Jambi, declined from 93 to 38% of provincial
63 area between 1977 and 2009 (Miettinen et al., 2012). These large scale transformations,
64 observed as land cover change, and land-use intensification have led to substantial losses in
65 animal and plant diversity, and ecosystem functions and changed microclimatic conditions
66 (Clough et al., 2016; Dislich et al., 2016; Drescher et al., 2016). Additionally, these changes
67 directly alter vegetation cover and structure as well as land surface properties such as albedo,
68 emissivity and surface roughness which affect gas and energy exchange processes between the
69 land surface and the atmosphere (Bright et al., 2015).

70

71 Replacing natural vegetation with another land cover modifies the surface albedo, which affects
72 the amount of solar radiation that is absorbed or reflected and consequently alters net radiation
73 and local surface energy balance. A low or high albedo results in smaller or greater reflection
74 of shortwave radiation. As a result the higher or lower amounts of net radiation absorption may
75 rise or lower the surface temperature and change evapotranspiration (Mahmood et al., 2014).

76

77 Changes in land cover also alter surface emissivity, i.e. the ratio of radiation emitted from a
78 surface to the radiation emitted from an ideal black body at the same temperature following the



79 Stefan–Boltzmann law. Emissivity of vegetated surfaces varies with plant species, density,
80 growth stage, water content and surface roughness (Snyder et al., 1998; Weng et al., 2004). A
81 change of emissivity affects the net radiation because it determines the emission of longwave
82 radiation that contributes to radiative cooling (Mahmood et al., 2014).

83

84 Water availability, surface type, soil humidity, local atmospheric and surface conditions affect
85 the energy partitioning into latent (LE), sensible (H) and ground heat (G) fluxes (Mildrexler et
86 al., 2011). Surface roughness affect the transferred sensible and latent heat by regulating vertical
87 mixing of air in the surface layer (van Leeuwen et al., 2011) thereby regulating land surface
88 temperature (LST). Through its association with microclimate, net radiation and energy
89 exchange (Coll et al., 2009; Sobrino et al., 2006; Voogt and Oke, 1998; Weng, 2009; Zhou and
90 Wang, 2011) LST is a major land surface parameter that also influences habitat quality and thus
91 the distribution of plants and animals and biodiversity.

92

93 The replacement of natural vegetation also changes evapotranspiration (ET) (Boisier et al.,
94 2014). In case ET is decreased, surface temperatures and fluxes of sensible heat (H) increase.
95 *Vice versa* when ET increases, increased LE fluxes lower surface temperatures and decrease H
96 fluxes (Mahmood et al., 2014). Vegetation structure as reflected by parameters such the
97 Normalized Difference Vegetation Index (NDVI), Leaf Area Index (LAI) and vegetation height
98 is in this respect an important determinant of the resistances or conductivities to heat, moisture,
99 and momentum transfer between the canopy and the atmosphere (Bright et al., 2015) facilitating
100 the amounts/ratios of sensible heat to water vapour dissipation away from the surface
101 (Hoffmann and Jackson, 2000).

102

103 Surface albedo, surface temperature, surface emissivity, and indirectly LAI and NDVI are
104 interconnected through the surface radiation balance. When the land surface is changed



105 feedback mechanisms involving these biophysical variables control the radiation balance and
106 the surface temperature.

107 To understand the effects of land cover changes on LST, the associated biophysical variables
108 must be evaluated. This can be done through the surface radiation budget and energy
109 partitioning which unites these biophysical variables directly or indirectly: albedo as direct
110 determinant of the net solar radiation, NDVI as a vegetation parameter determining the
111 emissivity which in turn determines the amount of reflected and emitted longwave radiation,
112 LST directly affecting the amount of emitted longwave radiation from the surface and ET
113 affecting the amount of energy that is used for surface cooling via evaporating of water.

114

115 The effect of land cover change on LST is dependent on the scale, location, direction and type
116 of the change (Longobardi et al., 2016). Several studies showed an increase of the LST after
117 forest were converted: in China built-up areas and agricultural land (Zhou and Wang, 2011),
118 and in crop land and pasture lands (Peng et al., 2014). Similar findings were reported for South
119 American ecosystems: low vegetation such as grasslands in Argentina were warmer than tall
120 tree vegetation (Nosetto et al., 2005). In Brazil, the surface temperature increased after the
121 conversion of natural Cerrado vegetation (a savanna ecosystem) into crop/pasture (Loarie et al.,
122 2011a). Similar effects were also shown for other South American biomes (Salazar et al., 2016).
123 In a global analysis, Li et al. (2015) showed that the cooling of forests is moderate at mid
124 latitudes and that Northern boreal forests are even warmer, an indication that the effect of land
125 cover change on LST varies with the location of the land cover change (Longobardi et al.,
126 2016). Similar studies on the Indonesian Islands are lacking but increases in surface temperature
127 are expected as an effect of the expansion of oil palm and cash crop land in the recent decades.

128

129 Measuring changes in LST is critical for understanding the effects of land cover changes, but
130 challenging. LST can be monitored with LST products retrieved from thermal infrared (TIR)



131 remote sensing data e.g. the use of the thermal bands of the Moderate Resolution Imaging
132 Spectrometer (MODIS) onboard the Terra and Aqua satellite (Sobrino et al., 2008), the thermal
133 band of the Thematic Mapper (TM) onboard the LANDSAT-5 platform (Sobrino et al., 2004,
134 2008) or Enhanced Thematic Mapper (ETM+) onboard the LANDSAT-7 platform. The
135 advantage of MODIS data is the availability of readily processed products at high temporal
136 resolution (daily) at medium (250 – 500 m) to coarse spatial resolution (1000 – 5000 m) scale;
137 MODIS LST product (MOD11A1/MYD11A1) for example is provided at a daily temporal
138 resolution with a spatial resolution of 1 km. Landsat data are provided at a higher spatial
139 resolution (30 m), but its temporal resolution is however limited to 16 days and the retrieval of
140 LST requires the correction of the satellite observed radiances for atmospheric absorption and
141 emission (Coll et al., 2009). Besides LST, the connected biophysical variables of the energy
142 and radiation budget can be derived from the visible and near-infrared (VIS-NIR) bands of
143 either MODIS or Landsat, making integrated monitoring of the biophysical variables related to
144 changing land surface possible. In Indonesia, a large proportion of the land use changes is
145 driven by small holders (Dislich et al. 2016), thus a combination of Landsat (for a fine spatial
146 resolution) and MODIS (for temporal developments) seems desirable.

147

148 The modification of the physical properties of the land surface influences climate/local
149 microclimatic conditions via biogeochemical and biophysical processes. Therefore, given
150 Indonesia's history of large scale agricultural land conversion and governmental plans to
151 substantially expand the oil palm production, it is important to study the effect of the expansion
152 of cash crop areas on the biophysical environment, especially on LST as a key land surface
153 parameter. These effects have been poorly studied in this region and according to our
154 knowledge this is the first study to quantify the effects of land use change on LST in Indonesia
155 We focus on the province of Jambi / Sumatra as it experience large land transformation towards



156 oil palm and other cash crops such as rubber plantations in the past and may serve as example
157 of future changes in other regions.

158

159 Our main objective is to quantify the differences in LST across different land cover types and
160 to assess the impact of cash crop expansion on the surface temperature of Jambi province (on
161 Sumatra / Indonesia) in the past decades. With this study we aim to (1) evaluate the use of
162 Landsat and MODIS satellite data as sources for a reliable estimation of the surface temperature
163 in a tropical region with limited satellite data coverage by comparing the surface temperatures
164 retrieved from both satellite sources to each other and against ground observations, (2) to
165 quantify the LST variability across different land cover types and (3) the long term effects of
166 land transformation on the surface temperature against the background of climatic changes and
167 (4) to identify the mechanisms that explain changes of the surface temperature through changes
168 in other biophysical variables. In this study we compare the surface temperatures of different
169 land cover types that replace forests (i.e. oil palm, rubber and acacia plantations, clear cut land
170 and urban areas) using high resolution Landsat and medium resolution MODIS satellite data
171 and discuss the differences by taking into account other biophysical variables such as the
172 albedo, NDVI and evapotranspiration (ET).

173

174 **2 Materials and methods**

175

176 **2.1 Study area**

177

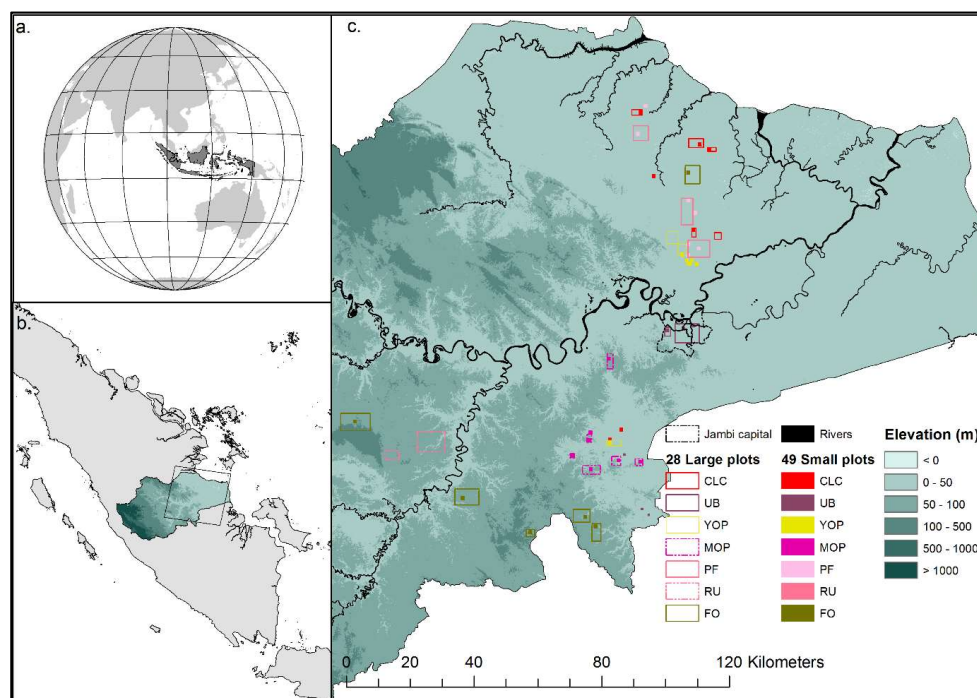
178 The study was carried out in the lowlands (approx. 25 000 km²) of the Jambi province (total
179 area 50 160 km²) on Sumatra, Indonesia, between latitudes 0°30'S and 2°30'S and longitudes
180 101°E and 104°30'E (Fig. 1). This region has undergone large land transformation towards oil
181 palm and rubber plantation over the past decades and thus may serve as an example of expected



182 changes in other regions of Indonesia (Drescher et al. 2016). The area has a humid tropical
183 climate with a mean annual temperature of 26.7 ± 0.2 °C (1991 – 2011, annual mean \pm SD of
184 the annual mean), with little intra-annual variation. Mean annual precipitation was 2235 ± 381
185 mm and a dry season with less than 120 mm monthly precipitation usually occurred between
186 June and September (Drescher et al., 2016). Details about the study area can be found in
187 (Drescher et al., 2016).

188

189 For this study, we used two data sets of different plot sizes. For the first data set, we delineated
190 28 large plots (ranging from 4 to 84 km²) of 7 different land cover types (Forest (FO), Rubber
191 (RU), Acacia Plantation Forest (PF), Young oil palm plantation (YOP), Mature Oil Palm
192 Plantation (MOP), Urban area (UB) and Clear Cut areas (CLC)) (Fig. 1). The delineation was
193 based on visual interpretation in combination with information from field work, which was
194 carried out between October – December 2013. The large size of the plots was necessary to
195 make a comparison between MODIS and Landsat images (see section satellite data). For the
196 second data set, we selected within and outside these 28 large plots 49 smaller plots (between
197 50 × 50 m and 1000 × 1000 m) (Fig. 1) which allowed us to increase the number of plots to use
198 when analysing Landsat images. These small plots were used to extract surface temperature
199 (LST), Normalized Difference Vegetation Index (NDVI), albedo (α) and evapotranspiration
200 (ET) from a high resolution Landsat satellite image (see section satellite data) for the 7 different
201 land cover types of interest.



202
203 **Fig. 1** Geographic location of the study area. Jambi province on the Sumatran Island of
204 Indonesia (Figs. 1a and 1b). The background of the map (Fig. 1c) is a digital elevation model,
205 showing that the plots are located in the lowlands of the Jambi province. The large rectangles
206 are the 28 different land cover types (Forest, Young and Mature Oil palm, Rubber, Urban area,
207 Acacia Plantation Forest and Clear Cut land), the small squares are the locations of the 49 small
208 plots of the 7 different land cover types. Abbreviations: CLC = Clear cut land, UB = Urban
209 area, YOP = Young oil palm plantation, MOP = Mature Oil Palm plantation, PF = Acacia
210 plantation forest, RU = Rubber plantation, FO = Forest.

211

212 **2.2 Meteorological data**

213

214 Air temperature and relative air humidity were measured at four reference meteorological
215 stations located in open areas within the area of study (Drescher et al., 2016), with
216 thermohygrometers (type 1.1025.55.000, Thies Clima, Göttingen, Germany) placed at 2m
217 height. Measurements were taken every 15 s and then averaged and stored in a DL16 Pro data



218 logger (Thies Clima, Göttingen, Germany) as 10 min mean, from February 2013 to December
219 2015. We used the air temperature from the meteorological stations to compare to MODIS air
220 temperatures (MOD07_L2). The relative air humidity was used as an input parameter for
221 NASA's online atmospheric correction (ATCOR) parameter tool to derive parameters to correct
222 Landsat thermal band for atmospheric effects (see Satellite data). We also used air temperature
223 and relative humidity from two eddy covariance flux towers located in the study area (Meijide
224 et al., 2017) one in a young oil palm plantation (two years old, S 01°50.127', E 103°17.737'),
225 and the other one in a mature oil palm plantation (twelve years old, S 01°41.584', E
226 103°23.484'). At these flux towers, air temperature and relative humidity were measured above
227 the canopy respectively with the same instruments as in the reference meteorological stations
228 (see Meijide et al. (2017), for description of methodology). In the flux tower located in the
229 mature oil palm plantation, we also measured surface canopy temperature between August 2014
230 and December 2015, which was compared to MODIS LST estimates from the same period.
231 Measurements of canopy temperature were performed with two infrared sensors (IR100)
232 connected to a data logger, (CR3000) both from Campbell Scientific Inc. (Logan, USA). For a
233 regional coverage we used ERA Interim daily air temperature grids
234 (<http://apps.ecmwf.int/datasets/data/interim-full-daily/levtype=sfc/>; (Dee et al., 2011) from
235 2000 – 2015 at 0.125 degrees resolution to study the annual air temperature trend in this period.

236

237 **2.3 Satellite data**

238

239 A Landsat 7 ETM+ VIS/TIR 30 m resolution surface reflectance image with low cloud cover,
240 acquired at 10:13 hours (local time) on 19 June 2013 covering the lowland area of the Jambi
241 province (path 125, row 61) was used in this study. Like all Landsat 7 ETM+ images acquired
242 after 31 may 2003, the image we used was affected by a scan line error causing a data loss of
243 about 22% (http://landsat.usgs.gov/products_slcoffbackground.php). Most selected plots were



244 located in the center of the image and thus not affected by the data loss, e.g. the forest plots
245 located at the edges of the scan line error zone faced minimal data loss because they were large
246 enough.

247 We also downloaded the tile h28v09 of the MODIS Terra (MOD) and Aqua (MYD) daily 1km
248 Land Surface Temperature and Emissivity products (MOD11A1 and MYD11A1 Collection-5)
249 and MODIS 16-days 500 m Vegetation Indices NDVI/EVI product (MOD13A1 Collection-5)
250 from 05 March 2000 till 31 December 2015 for Terra data and from 8 July 2002 till 31
251 December 2015 for Aqua data. We downloaded other supporting satellite data such as the
252 MODIS Atmospheric Profile product (MOD07_L2) and the MODIS Geolocation product
253 (MOD03). All MODIS data were reprojected to WGS84, UTM zone 48 South using the MODIS
254 Reprojection Tool (MRT). The quality of the MODIS data was checked using the provided
255 quality flags and only pixels with the highest quality flag were used in the analysis.

256

257 **2.4 Retrieval of biophysical variables from Landsat 7 ETM+ VIS/TIR images**

258

259

- 260 • *NDVI*

261

262 NDVI was derived using the reflectances corrected for atmospheric effects in the red (ρ_{RED} ,
263 band 3 Landsat 7 ETM+) and near infrared (ρ_{NIR} , band 4 Landsat 7 ETM+) bands, with:

264

265

$$266 \quad NDVI = \frac{\rho_{\text{NIR}} - \rho_{\text{RED}}}{\rho_{\text{NIR}} + \rho_{\text{RED}}} \quad (1)$$

267

268 • *Surface albedo*

269

270 The surface albedo (α) was computed using the equation of Liang (2000) for estimating
271 broadband albedo from Landsat surface reflectance bands, with:

272

$$273 \alpha = 0.3141 \rho_1 + 0.1607 \rho_3 + 0.369 \rho_4 + 0.1160 \rho_5 + 0.0456 \rho_7 - 0.0057 \quad (2)$$

274

275 where ρ_1 , ρ_3 , ρ_4 , ρ_5 and ρ_7 are the Landsat 7 ETM+ surface reflectance bands (corrected for
276 atmospheric effects).

277

278 • *Surface temperature (LST)*

279

280 LST was derived following the method proposed by Bastiaanssen (2000), Bastiaanssen et al.
281 (1998a), Coll et al. (2010) and Wukelic et al. (1989) for computing the surface temperature
282 from the thermal infrared band (TIR, band 6) of Landsat (Supporting information, S1). The
283 thermal infrared band (TIR, band 6) was first converted to thermal radiance (L_6 , $W/m^2/sr/\mu m$)
284 and then to atmospherically corrected thermal radiance (R_c , $W/m^2/sr/\mu m$) following the method
285 described by Wukelic et al. (1989) and Coll et al. (2010), and using the atmospheric parameters
286 obtained on NASA's online Atmospheric Correction Calculator (Barsi et al., 2003, 2005)
287 (supporting information, S2). The surface temperature (LST, °K) was computed through the
288 following equation similar to the Planck equation, as in Coll et al. (2010) and Wukelic et al.
289 (1989):

290



$$291 \quad LST = \frac{k_2}{\ln\left(\frac{\epsilon_{NB} \cdot k_1}{R_c} + 1\right)} \quad (3)$$

292

293 where ϵ_{NB} is the emissivity of the surface obtained from the NDVI (Supporting information,
294 Table S1), k_1 (= 666.09 mW/cm²/sr/μm) and k_2 (= 1282.71 °K) are sensor constants for
295 converting the thermal radiance obtained from band 6 of Landsat 7 to surface temperature.

296 The surface temperature derived from Landsat thermal band was compared with a MODIS LST
297 product that was acquired on the same day at 10:30 am local time. For this, the Landsat LST
298 image was resampled to MODIS resolution to enable a pixel to pixel comparison, followed by
299 extracting the average LST of 7 land cover types using the data set containing the large
300 delineated plots (Fig. 1).

301

- 302 • *Evapotranspiration (ET)*

303

304 Based on the Surface Energy Balance Algorithm for Land (SEBAL) (Bastiaanssen, 2000;
305 Bastiaanssen et al., 1998a, 1998b) we estimated ET (mm/hr) from latent heat fluxes (LE, W/m²)
306 which were computed as the residual from sensible (H, W/m²) and ground (G, W/m²) heat
307 fluxes subtracted from net radiation (R_n, W/m²) as:

308

$$309 \quad LE = R_n - G - H \quad (4)$$

310

311 We calculated R_n as the sum of incoming shortwave and longwave radiation, minus the
312 reflected shortwave and longwave radiation and the emitted longwave radiation (equation 5).

313 The surface albedo, surface emissivity and surface temperature determine the amounts of
314 incoming and reflected radiation:

315



$$316 \quad R_n = (1 - \alpha) S_{d\downarrow} + \varepsilon_a \sigma T_a^4 - (1 - \varepsilon_0) \varepsilon_a \sigma T_a^4 - \varepsilon_0 \sigma LST^4 \quad (5)$$

317

318 Where $S_{d\downarrow}$ is the incoming shortwave solar radiation (W/m^2) at the surface; α is the surface
 319 albedo (equation 2); ε_0 is the surface emissivity (-); ε_a is the atmospheric emissivity (-); σ is the
 320 Stephan-Boltzmann constant ($5.67 \times 10^{-8} W/m^2/K^4$); LST is the surface temperature (K,
 321 equation 3); T_a is the near surface air temperature (K). The surface emissivity (ε_0) is derived
 322 from the NDVI and is described in the supporting information (Table S1). The average
 323 atmospheric emissivity (ε_a) is estimated with the model of Idso and Jackson, (1969):

324

$$325 \quad \varepsilon_a = 1 - 0.26 \cdot \exp \{(-7.77 \times 10^{-4}) \cdot (273.15 - T_a)^2\} \quad (6)$$

326

327 Ground heat fluxes (G , W/m^2) were derived as a fraction of R_n from an empirical relationship
 328 between LST, α , and NDVI (Bastiaanssen, 2000) as:

329

$$330 \quad G = R_n \cdot \frac{LST - 273.15}{\alpha} \cdot (0.0038\alpha + 0.0074\alpha^2) \cdot (1 - 0.98NDVI^4) \quad (7)$$

331

332 In SEBAL Sensible heat flux (H , W/m^2) was calculated as:

333

$$334 \quad H = \rho C_p \frac{\Delta T}{r_{ah}} = \rho C_p \frac{a LST + b}{r_{ah}} \quad (8)$$

335

336 Where ρ is the air density ($1.16 kg/m^3$); C_p is the specific heat of air at constant pressure (1004
 337 $J/kg/K$); r_{ah} is the aerodynamic resistance to heat transport ($s m^{-1}$); a and b are regression
 338 coefficients which are determined by a hot extreme pixel (where $LE = 0$ and H is maximum)
 339 and a cold extreme pixel (where $H = 0$ and LE is maximum). The aerodynamic resistance to
 340 heat transport, r_{ah} , is calculated through an iterative process with air temperature measured at 2



341 m as input. SEBAL is described in Bastiaanssen (2000) and Bastiaanssen et al. (1998a, 1998b).
342 The application of SEBAL in this research is briefly described in the supporting information
343 (S3: ET from satellite images).

344

345 **2.5 Local short term differences between different land cover types**

346

347 From the created LST, NDVI, Albedo and ET images we extracted the average values of the
348 different land cover classes. For this we used the dataset containing the small 49 delineated
349 plots covering 7 different land cover types (Fig. 1). The average effect of land transformation,
350 i.e. the change from forest to another non-forest land cover type, on the surface temperature
351 was evaluated as (cf. Li et al. (2015)) :

352

$$353 \Delta LST = LST_{\text{non-forest}} - LST_{\text{forest}} \quad (1)$$

354

355 A negative ΔLST indicates a cooling effect and positive ΔLST indicates a warming effect of
356 the non-forest vegetation compared to forest. The same procedure was applied in evaluating the
357 effect of land transformation on the NDVI, albedo and ET.

358

359 **2.6 Effects of land cover change on the provincial surface temperature in the past decades**

360

361 To analyse the long term effects on the provincial scale we used the MODIS daily LST time
362 series (MOD11A1 and MYD11A1) from 2000 – 2015. MOD11A1 provides LST for two times
363 of the day: 10:30 am and 10:30 pm and we used the times series between 2000 and 2015.
364 MYD11A1 provides LST for 1:30 am and 1:30 pm and is available from 8 July 2002; we used
365 complete years in our analysis and therefore used the MYD11A1 time series from 2003 – 2015.
366 We calculated the mean annual LST at four different times of the day (10:30 am, 1:30 pm,



367 10:30 pm and 1:30 am) between 2000 and 2015 for the lowland of the Jambi from the MODIS
 368 daily LST time series (MOD11A1 and MYD11A1). To do so (1) we calculated for each pixel
 369 the average LST pixel value using only the best quality pixels for every year; (2) from these
 370 pixels we made a composite image ($n = 16$, one for each year) for the province and (3) from
 371 each composite image we calculated the mean annual lowland provincial temperature as the
 372 average of all the pixels that are enclosed by a zone delineating the lowland of the Jambi
 373 province. We performed the same analysis with the MODIS 16-day NDVI product (2000 –
 374 2015) and the ERA daily temperature grid (2000 – 2015) to compare the annual trends of LST,
 375 NDVI and air temperature of the province. The average provincial LST and NDVI were
 376 compared to the mean LST and NDVI of a selected forest that remained undisturbed forest
 377 during the 2000 – 2015 period.

378

379 2.7 Statistical analysis

380

381 For comparison of the Landsat derived LST and the MODIS LST we analyzed the statistical
 382 relationships with the coefficient of determination (R^2), the root mean square error (RMSE),
 383 the mean absolute error (MAE) and the bias (Bias):

$$384 \text{ RMSE} = \sqrt{\frac{\sum_{i=1}^N (E_i - O_i)^2}{N}} \quad (9)$$

385

$$386 \text{ Bias} = \frac{\sum_{i=1}^N (E_i - O_i)}{N} \quad (10)$$

387

$$388 \text{ MAE} = \frac{\sum_{i=1}^N |E_i - O_i|}{N} \quad (11)$$

389



390 Where O_i is MODIS LST, E_i is the Landsat surface temperature, and N is the number of pixels
391 compared. Model type 2 linear regression was applied for fitting the relation between MODIS
392 LST and Landsat LST.

393 We tested the relation between the biophysical variables LST (or L6 and Rc, both as pre- or
394 intermediate products before obtaining LST), albedo (α), NDVI and ET with correlation
395 analysis and a multiple linear regression was applied to analyse the effects of the biophysical
396 variables on the LST. We used the model: LST (or Rc or L6) $\sim \alpha + NDVI + ET$, and used R^2
397 and standardized β -coefficients to evaluate the strength of the biophysical variables in
398 predicting the LST.

399

400 **3 Results**

401

402 **3.1 Landsat LST compared to MODIS LST**

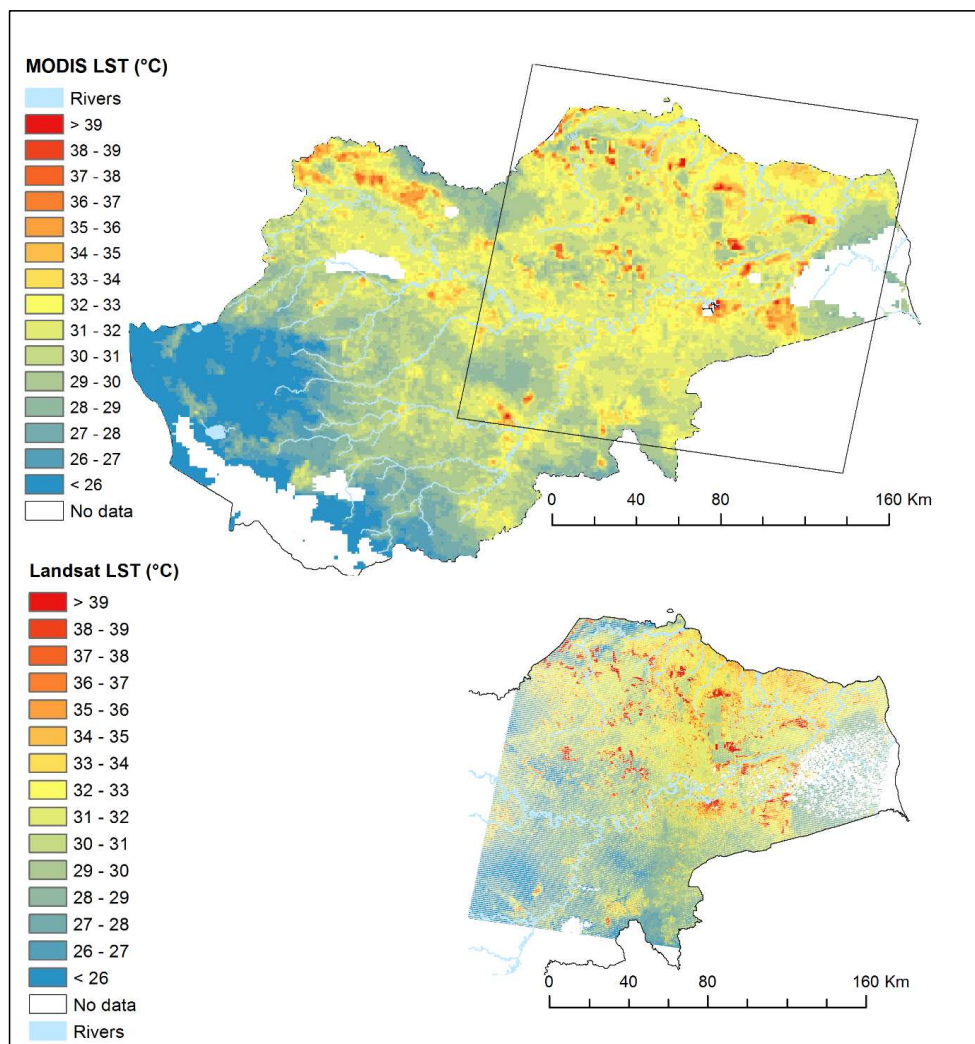
403

404 Landsat and MODIS images showed similar spatial patterns of LST(Fig. 2). In both images the
405 hot areas correspond to the known clear cut areas, urban areas or other sparsely vegetated areas,
406 the cooler areas correspond to vegetated areas such as forest, plantation forests and mature oil
407 palm plantations. The coarse resolution scale of MODIS (1000 m for LST) allows a large
408 regional coverage of the study area but does not allow to retrieve detailed information on small
409 patches (smaller than 1 km²). On the other hand, Landsat 7 image allows a detailed study of
410 patches that are small enough (as small as 30 x 30 m²), but is affected by the scan line error
411 causing data loss at the edges of the image. In both MODIS and Landsat images clouds and
412 cloud shadows were removed and therefore lead to data gaps in the images.

413

414

415



416
417
418

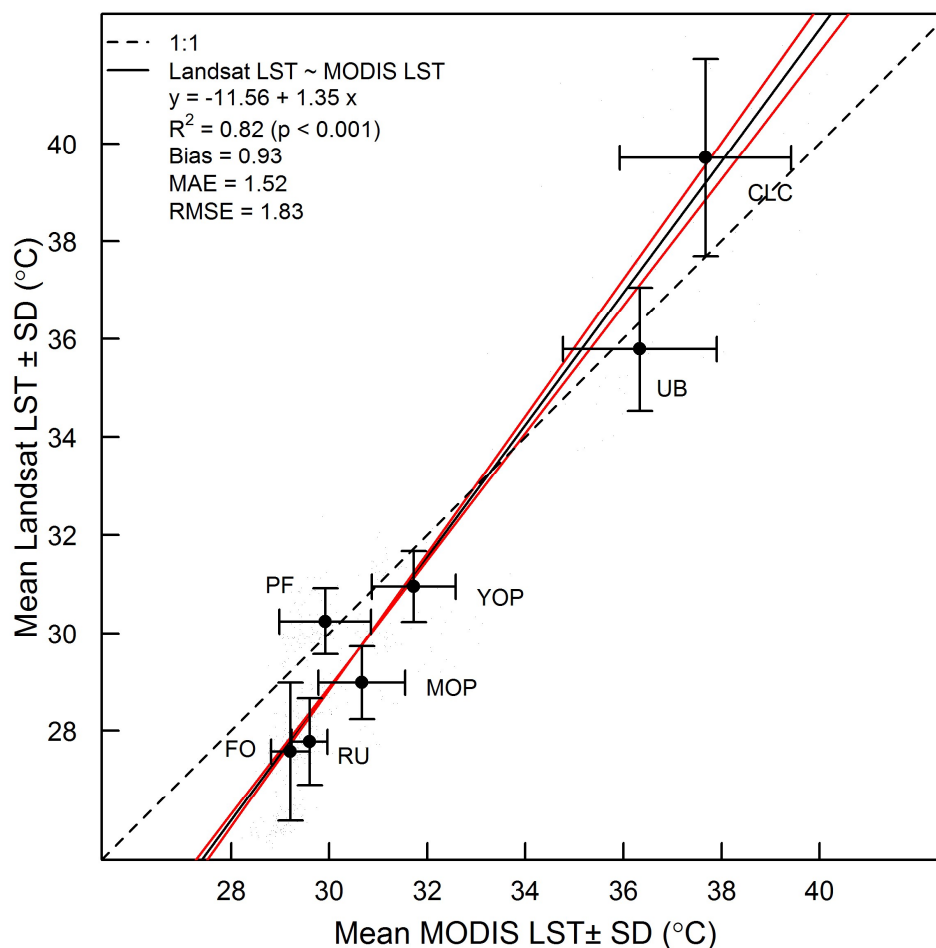
419 **Fig. 2** MODIS LST image (top) compared with Landsat LST image (bottom). Cloud cover and
420 cloud shadow cover resulted in data gaps (No data). The difference in acquisition time between
421 the images is 15 minutes. The square in the MODIS image is the area that is covered by the
422 Landsat tile (path 125, row 61). Both satellite images were acquired on 19 June 2013.

423

424 Landsat derived LST correlated well with MODIS LST ($R^2 = 0.82$; $p < 0.001$; Fig. 3) with a
425 RMSE of 1.83 °C. The 7 land cover types had distinctive LSTs and the observed differences



426 between these land cover types were consistent in both images. The non-vegetated surfaces
427 (Clear cut land (CLC) and Urban areas (UB)) had higher surface temperatures than the
428 vegetated surface types (FO, YOP, MOP, PF and RU). Clear cut land had the highest surface
429 temperature of all compared land cover types, followed by urban areas whereas the vegetated
430 land cover types had lower surface temperatures: $LST_{CLC} (39.71 \pm 2.01 \text{ }^{\circ}\text{C}) > LST_{UB} (35.79 \pm$
431 $1.26 \text{ }^{\circ}\text{C}) > LST_{YOP} (30.95 \pm 0.72 \text{ }^{\circ}\text{C}) > LST_{PF} (30.25 \pm 0.67 \text{ }^{\circ}\text{C}) > LST_{MOP} (28.98 \pm 0.75 \text{ }^{\circ}\text{C})$
432 $> LST_{RU} (27.78 \pm 0.89 \text{ }^{\circ}\text{C}) > LST_{FO} (27.57 \pm 1.41 \text{ }^{\circ}\text{C})$ (Landsat LST, Fig. 3). The same trend
433 was derived from the MODIS image but with higher surface temperatures, except for CLC:
434 $LST_{CLC} (37.67 \pm 1.75 \text{ }^{\circ}\text{C}) > LST_{UB} (36.33 \pm 1.57 \text{ }^{\circ}\text{C}) > LST_{YOP} (31.73 \pm 0.85 \text{ }^{\circ}\text{C}) > LST_{MOP}$
435 $(30.67 \pm 0.88 \text{ }^{\circ}\text{C}) > LST_{PF} (29.92 \pm 0.93 \text{ }^{\circ}\text{C}) > LST_{RU} (29.60 \pm 0.36 \text{ }^{\circ}\text{C}) > LST_{FO} (29.21 \pm 0.40$
436 $^{\circ}\text{C})$ (MODIS LST, Fig. 3).



437
 438 **Fig. 3** Average surface temperature (LST) and standard deviation (SD) of 7 land cover types
 439 derived from Landsat thermal image compared with the mean and SD of MODIS LST.
 440 CLC = Clear cut land, UB = Urban areas, YOP = young oil palm plantation, PF = Acacia
 441 Plantation Forest, MOP = Mature Oil palm plantation, FO = Forest, RU = Rubber plantation.
 442 The dashed line is the theoretical 1:1 line, the solid lines are the Linear Model type 2 regression
 443 line (black) and the confidence limits of the regression line (red). Landsat and MODIS images
 444 were acquired on 19 June 2013, Landsat at 10:13 am local time, MODIS at 10:30 am local time.
 445 Landsat pixels (30 m) were resampled to MODIS pixel resolution (926 m) to make a pixel to



446 pixel comparison between the two sources possible. RMSE is the root mean squared error, MAE
447 is mean absolute error.

448

449 **3.2 Local short term differences between different land cover types**

450

451 The Δ LST between RU, MOP, PF, YOP, UB and CLC land cover types and FO were all
452 positive, meaning that all other land cover types were warmer than forests (Fig. 4a & Supporting
453 Information S4 and S5). RU and MOP were 0.4 ± 1.5 °C and 0.8 ± 1.2 °C warmer than forest,
454 respectively. PF and YOP were much warmer than forests (Δ LST_{PF-FO} = 2.3 ± 1.1 °C, Δ LST_{YOP}
455 _{-FO} = 6.0 ± 1.9 °C). The largest Δ LSTs were between forest and the non-vegetated land cover
456 types, i.e. UB (Δ LST = 8.5 ± 2.1 °C) and CLC (Δ LST = 10.9 ± 2.6 °C). The LST differences
457 were significant ($p < 0.05$, post-hoc Tukey's HSD test), except between RU and FO ($p = 0.78$,
458 post-hoc Tukey's HSD test (Supporting Information S6, Table S6.1 & table S6.2).

459

460 Similar differences were found for the Δ NDVI between forest and other land covers (Fig. 4b).

461 The negative Δ NDVI indicates that the non-forest land cover types had lower NDVI than forest.
462 Δ NDVI between FO and RU, MOP, PF and YOP were small (between -0.01 ± 0.02
463 (Δ NDVI_{MOP-FO}) and -0.12 ± 0.06 (Δ NDVI_{YOP-FO}). The largest Δ NDVIs were between forest
464 and the non-vegetated land cover types, i.e. UB and CLC (Δ NDVI = -0.42 ± 0.11 and -0.41
465 ± 0.08 , respectively). All Δ NDVIs were significant ($p < 0.05$, post-hoc Tukey's HSD test).

466

467 The difference in albedo (Δ Albedo) between forest and the other land covers was very small
468 (Fig. 4c), with Δ Albedo values between -0.03 ± 0.01 (Δ Albedo_{PF-FO}) and 0.03 ± 0.02
469 (Δ Albedo_{YOP-FO}). These differences were significant ($p < 0.05$, post-hoc Tukey's HSD test).
470 PF had a lower albedo than forest (Δ Albedo_{PF-FO} = -0.03 ± 0.01), while the other land cover
471 types had a higher albedo than forest.

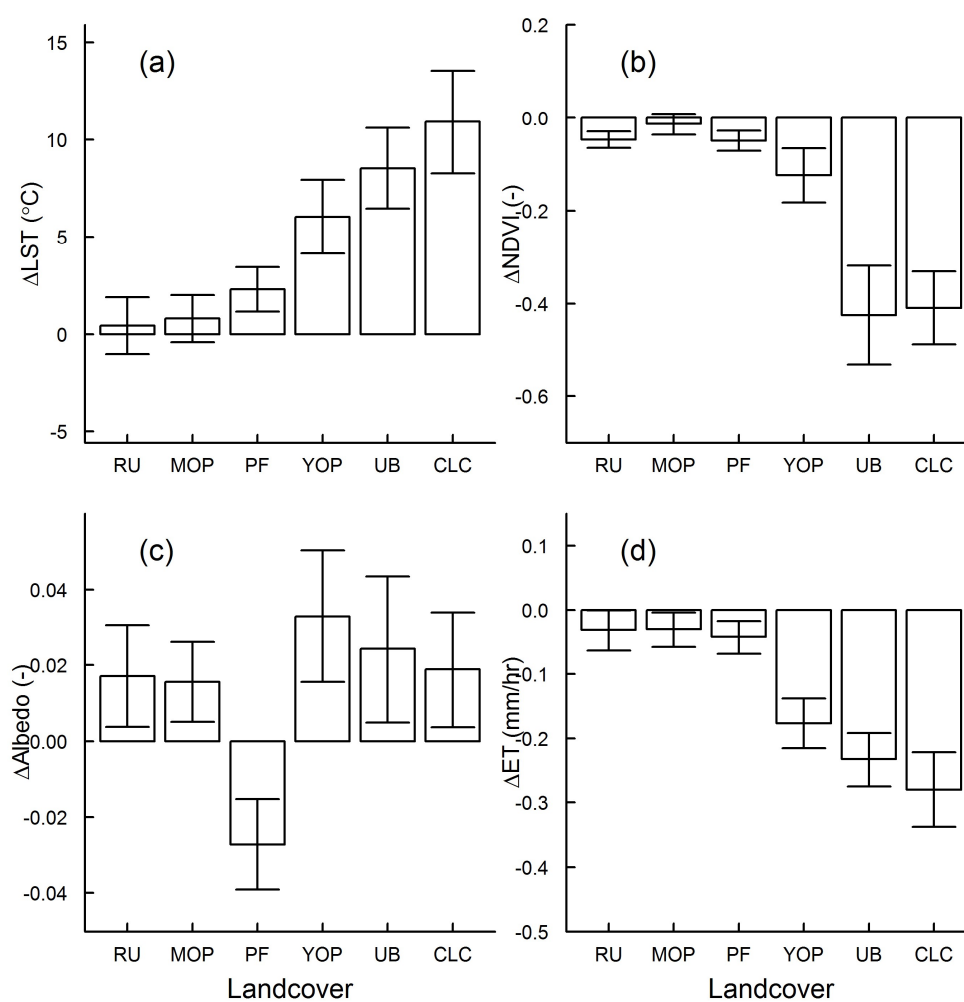


472

473 All land covers had lower ET than forest. RU, MOP and PF had slightly lower ET than FO

474 ($\Delta ET_{RU-FO} = -0.03 \pm 0.04$, $\Delta ET_{MOP-FO} = -0.03 \pm 0.03$ mm/hr, $\Delta ET_{PF-FO} = -0.04 \pm 0.03$ mm/hr)475 (Fig. 4d). YOP, UB and CLC had much lower ET values than forests: $\Delta ET_{YOP-FO} = -0.18 \pm$ 476 0.04 mm/hr, $\Delta ET_{UB-FO} = -0.23 \pm 0.04$ mm/hr, $\Delta ET_{CLC-FO} = -0.26 \pm 0.06$ mm/hr). The ΔET s477 were significant ($p < 0.05$, post-hoc Tukey's HSD test).

478



479

480 **Fig. 4** Differences (mean \pm SD) in surface temperature (ΔLST), normalized difference481 vegetation index ($\Delta NDVI$), Albedo ($\Delta Albedo$) and Evapotranspiration (ΔET) between other



482 land covers (RU, MOP, PF, YOP, UB and CLC) and forest (FO) in the Jambi province, derived
 483 from the Landsat LST image acquired on 19 June 2013 at 10:13 am local time.

484

485 Albedo had the weakest influence on the LST ($\rho = 0.25$, $p < 0.05$) (Table 2) than NDVI and
 486 ET. As the thermal radiance band (L6) and the atmospherically corrected thermal band (Rc)
 487 were the basis for the LST calculation, the high correlation between L6 and NDVI ($\rho = -0.87$,
 488 $p < 0.05$) and between L6 and ET ($\rho = -0.98$, $p < 0.05$) resulted in a high correlation between
 489 LST and NDVI ($\rho = -0.88$) and between LST and ET ($\rho = -0.98$). The analysis showed that
 490 albedo, NDVI and ET were all significant predictors of LST ($F_{(3, 41586)} = 1 \times 10^6$, $p < 0.05$). ET
 491 was the strongest predictor of LST (stand. $\beta = -1.11$, $p < 0.05$). Albedo (stand. $\beta = -0.19$, $p <$
 492 0.05 , resp.) and NDVI (stand. $\beta = -0.19$, $p < 0.05$) were weaker predictors of LST.

493

494 **Table 2** Statistical analysis between biophysical variables (albedo (α), NDVI and ET) and
 495 Spectral Radiance band (L6), corrected thermal band (Rc) and Landsat surface temperature
 496 (LST).

Model		ρ	R^2	β	Stand. β	Model fit (R^2)	F-statistics
L6 ~ α + NDVI + ET	α	0.26	0.05	-2.94	-0.19	0.99	F (3, 41586) = 1.10×10 ⁶ , ***
	NDVI	-0.87	0.10	0.23	0.11		
	ET	-0.98	1.13	-4.00	-1.16		
Rc ~ α + NDVI + ET	α	0.25	0.05	-4.88	-0.20	0.99	F (3, 41586) = 1.79×10 ⁶ , ***
	NDVI	-0.88	0.04	0.16	0.05		
	ET	-0.98	1.00	-6.21	-1.10		
LST ~ α + NDVI + ET	α	0.25	0.05	-34.01	-0.19	0.99	F(3, 41586) = 2.3×10 ⁶ , ***
	NDVI	-0.88	0.05	1.30	0.05		
	ET	-0.98	1.00	-43.53	-1.11		

497 ***. $p = 2 \times 10^{-16}$

498 LM: Multiple linear regression analysis between LST (or L6 or Rc) and 3 biophysical variables:
 499 Albedo (α), NDVI and ET. ρ = correlation coefficient; R^2 : R-squared of the components; β =
 500 regression coefficient of the component; stand. β = standardized β ; Model fit (R^2): overall model



501 fit of the multiple linear regression. The values in brackets are for the analysis between the
502 biophysical variables and the corrected thermal band (R_c).

503

504 A separate analysis (Table S6.3, Supporting information S6) showed that ET was a strong
505 predictor of LST for each land cover type in this study and that NDVI and albedo were minor
506 predictors of LST.

507

508 **3.3 Effects of land-use change on the provincial surface temperature in the past decades**

509

510 The average annual LST of the province was characterized by a fluctuating but increasing trend
511 during daytimes (Fig. 5a and 5b) between 2000 and 2015. The average morning LST (10:30
512 am) increased by 0.07 °C per year ($R^2 = 0.59$; $p < 0.0001$), the midday afternoon LST (13:30
513 local time) increased by 0.13 °C per year ($R^2 = 0.35$; $p = 0.02$) between 2003 and 2015. While
514 the daytime LST showed a clear increase, the night and evening LST (10:30 pm and 1:30 am,
515 Fig. 5c and 5d) trends were small showing a decrease of -0.02 °C ($R^2 = 0.29$; $p = 0.02$) and $-$
516 0.01 °C ($R^2 = 0.05$; $p = 0.51$) per year, respectively. The observed LST trends resulted in a total
517 LST increase of 1.05 °C and 1.56 °C in the morning (10:30 am) and afternoon (1:30 pm)
518 respectively and a total decrease of the province LST of 0.3 °C (10:30 pm) and 0.12 °C (1:30
519 am) at night over the time period 2000 to 2015.

520

521 In order to separate the effect of land use change from global climate warming, we used a site
522 constantly covered by forest over that period (from the forest sites we used in this study) as a
523 reference not directly affected by land cover changes. That site showed less changes in LST
524 than the entire province: only the mean morning LST (10:30 am) had a significant but small
525 trend with an increase by 0.03 °C per year ($R^2 = 0.21$, $p < 0.05$) resulting in a total LST increase
526 of the province of 0.45 °C between 2000 and 2015 (Fig. 5a). This LST warming is much smaller



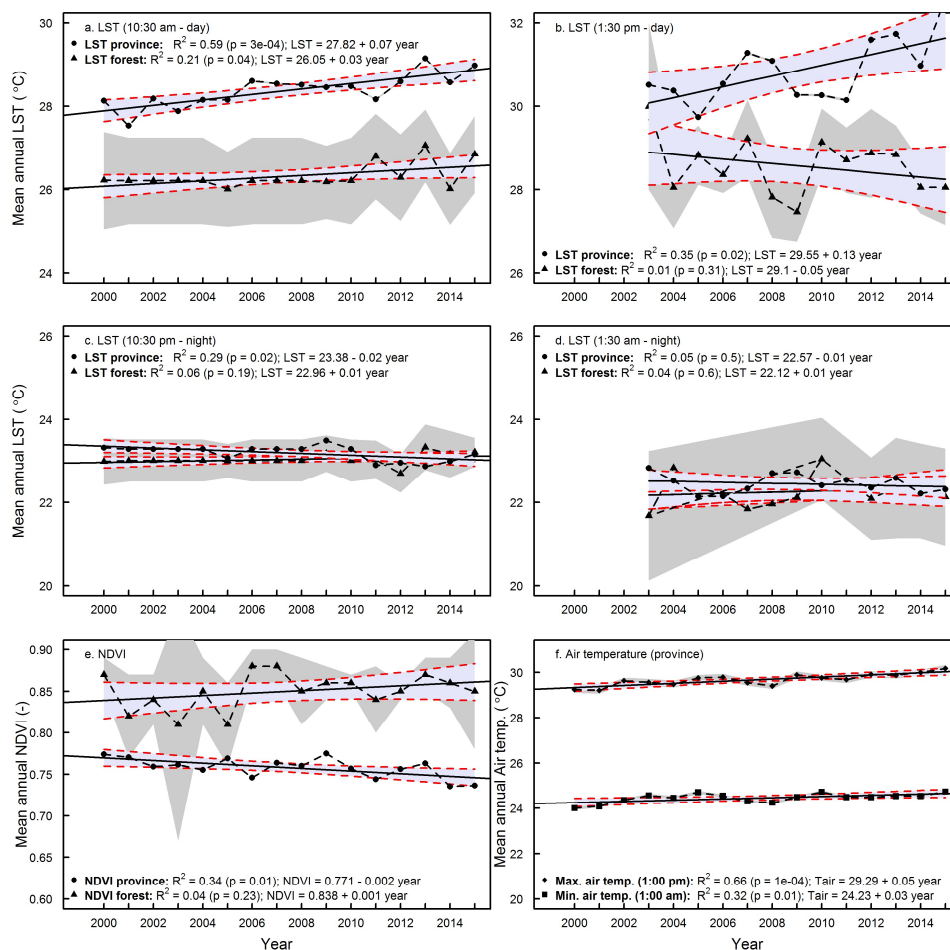
527 than the overall warming at provincial level of 1.05 °C. The LST time series at other times
528 showed no significant trends: the mean afternoon LST (1:30 pm) with -0.05 °C per year ($R^2 =$
529 0.01, $p = 0.31$) (Fig. 5b), the night and evening LST with 0.01°C per year (Fig. 5c and 5d, $p =$
530 0.19 and $p = 0.65$, respectively).

531

532 The mean annual NDVI of the province decreased by 0.002 per year which resulted in a total
533 NDVI decrease of 0.03 ($R^2 = 0.34$; $p = 0.01$; Fig. 5e). The NDVI of the forest showed a small
534 but not significant increase of 0.001 per year ($R^2 = 0.04$, $p = 0.23$) (Fig. 5e) fluctuating around
535 an NDVI of 0.84.

536

537 The mean annual midday air temperature (at 1:00 pm, local time, Fig. 5f) and the mean annual
538 night air temperature (at 1:00 am, local time) increased every year by 0.05 °C and 0.03 °C,
539 respectively resulting in a total air temperature increase of 0.75 °C ($R^2 = 0.66$, $p < 0.0001$) and
540 0.45 °C ($R^2 = 0.32$, $p = 0.014$) between 2000 and 2015 (Fig. 5f).



541
 542 **Fig 5.** Mean annual LST (a – d), mean annual NDVI (e) and mean annual air temperature trends
 543 (f) in the Jambi province between 2000 and 2015 derived from MODIS LST (5a. 10:30 am, 5b.
 544 1:30 pm, 5c. 10:30 pm and 5d. 1:30 am, local time), MODIS NDVI and ERA Interim Daily air
 545 temperature (1:00 am and 1:00 pm, local time) data sets respectively. Grey-shaded areas are the
 546 confidence intervals of the means, blue-shaded areas are the confidence intervals of the
 547 regression lines. MODIS LST time series for 1:30 pm and 1:30 am were available from the mid
 548 of 2002; for this reason we used the complete years from 2003 till 2015.

549

550 **4 Discussion**



551

552 **4.1 Landsat LST compared to MODIS LST**

553

554 In our study we retrieved the surface temperature from a Landsat image and compared this with
555 MODIS LST. Our results showed a good agreement between both LSTs (Fig. 3), which is
556 comparable to other studies and thus gives confidence in our analysis. Bindhu et al. (2013)
557 found also a close relationship between MODIS LST and Landsat LST using the same
558 aggregation resampling technique as our method and found R^2 of 0.90, a slope of 0.90, and an
559 intercept of 25.8 for LST, compared to our R^2 of 0.8, slope of 1.35 and intercept of -11.58 (Fig.
560 3). Zhang and He (2013) validated Landsat LST with MODIS LST and also found good
561 agreements (RMSD 0.71 – 1.87 °C) between the two sensors, where we found a RMSE of 1.71
562 °C. Nevertheless, there still are differences and slope versatility between the two satellite
563 sources. These differences are typically caused by differences between MODIS and Landsat
564 sensors in terms of (a) different sensor properties e.g. spatial and radiometric resolution and
565 sensor calibration; (b) geo-referencing and differences in atmospheric corrections (Li et al.,
566 2004); and (c) emissivity corrections i.e. the use of approximate equations to derive the
567 emissivity from the NDVI from Landsat's Red and NIR bands. Li et al. (2004) and Vlassova et
568 al. (2014) identified these same factors in their comparison of ASTER LST with MODIS LST
569 and Landsat LST with MODIS LST, respectively. Vlassova et al. (2014) found good
570 agreements between MODIS and Landsat LST with MODIS LST to be higher than Landsat
571 LST, which they attributed to the delay of 15 minutes in acquisition time between MODIS and
572 Landsat. MODIS LST is measured 15 minutes later and our results showed that MODIS LSTs
573 were indeed higher than Landsat LST. A comparison of MODIS LST with locally measured
574 canopy surface temperatures during the overpass time of MODIS also showed agreement
575 (Supporting information S7, Figure S7.1). The slope was possibly due to differences in



576 instrumentation and emissivity corrections and to scale issues, still this comparison could
577 corroborate the quality check of MODIS LST.

578 As the MODIS LST product is proven to be accurate within 1 °C (Silvério et al., 2015; Wan et
579 al., 2004) and has been intensively validated, the use of MODIS LST was a proper way to assess
580 the quality of our Landsat LST.

581

582 The errors from the different sources (such as atmospheric correction, emissivity correction,
583 resampling Landsat to MODIS resolution) are difficult to quantify. When we tested the impact
584 of atmospheric correction and emissivity errors on the LST from Landsat retrieval we found
585 that: (a) the overall patterns across different land use types did not change, (b) emissivity was
586 the most important factor but the effects on LST retrieval were small and (c) errors due to
587 atmospheric correction parameters were small because there were small differences between
588 default Atmospheric correction (ATCOR) parameters and ATCOR parameters derived with
589 actual local conditions (relative humidity (RH), air pressure and air temperature). Following
590 the method of Coll et al. (2009) and Jiang et al. (2015) we show that the use of the online
591 atmospheric correction parameter calculator is a good option provided that RH, air temperature
592 and air pressure are available. We additionally compared locally measured air temperatures
593 with MODIS air temperature and found a good agreement (Supporting information S8, Figure
594 S8.1), which served as a verification that we used a correct air temperature for the atmospheric
595 correction parameter calculator.

596 Overall, our comparison of LST from Landsat against LST from MODIS as well as against
597 ground observation suggests that we are able to retrieve meaningful spatial and temporal
598 patterns of LST in Jambi province.

599

600 **4.2 LST patterns across different LULC types**

601



602 The land cover types in our study covered a range of land surface types that develop after forest
603 conversion. This is the first study in this region that includes oil palm and rubber as land use
604 types that develop after forest conversion. The coolest temperatures were at the vegetated land
605 cover types while the warmest surface temperatures were on the non-vegetated surface types
606 like urban areas and bare land. Interestingly, the oil palm and rubber plantations were only
607 slightly warmer than the forests whereas the young oil palm plantations had clearly higher LST
608 than the other vegetated surfaces. For other parts of the world, Lim et al. (2005, 2008), Fall et
609 al. (2010) and Weng et al. (2004) also observed cooler temperatures for forests and the highest
610 surface temperatures for barren and urban areas.

611 In Indonesia, land transformation is often not instantaneous from forest to oil palm or rubber
612 plantation, but can be associated with several years of bare or abandoned land in-between (Sheil
613 et al., 2009). Oil palm plantation typically have a rotation cycle of 25 years, resulting in
614 repeating patterns with young plantations (Dislich et al., 2016). Given the large differences in
615 LST between forests and bare soils or young oil palm plantations that we observed, a substantial
616 warming effect of land transformation at regional scale is expected.

617

618

619 **4.3 Drivers of local differences between different land cover types**

620

621 All land cover types (except Acacia Plantation Forests) had a higher albedo than forest,
622 indicating that these land cover types absorbed less incoming solar radiation than forests.
623 Nevertheless, these land cover types were warmer than forests, suggesting that the albedo was
624 not the dominant variable explaining LST. Indeed, the statistical analysis showed that $ET \sim$
625 LST had a higher correlation than $albedo \sim LST$. The ΔETs were significant, underlying that
626 despite their higher albedo all land cover types had higher LSTs than forests due to lower ET
627 rates than forests. Vice versa, forests that absorb more solar radiation due to the lower albedo,



628 have lower LST due to the higher ET they exhibit, hereby identifying evaporative cooling as
629 the main determinant of regulating the surface temperature of all vegetation cover types (Li et
630 al., 2015).

631

632 Both observational and modeling studies carried out in other geographic regions and with other
633 trajectories support our observations. Observational studies in the Amazonia by Lawrence and
634 Vandecar (2015) on the conversion of natural vegetation to crop or pasture land showed a
635 surface warming effect. Salazar et al. (2015) provided additional evidence that conversion of
636 forest to other types of land use in the Amazonia cause significant reductions in precipitation
637 and increases in surface temperatures.

638 Alkama and Cescatti (2016) and earlier studies by Loarie et al. (2011a, 2011b) showed that
639 tropical deforestation may increase LST, croplands in the Amazonian regions were also warmer
640 than forests through the reduction of ET (Ban-Weiss et al., 2011; Feddema et al., 2005) and that
641 the climatic response strongly depends on changes in energy fluxes rather than on albedo
642 changes (Loarie et al., 2011a, 2011b). A study by Silvério et al. (2015) indeed found that
643 tropical deforestation changes the surface energy balance and water cycle and that the
644 magnitude of the change strongly depends on the land uses that follow deforestation. They
645 found the LST over croplands 6.4 °C higher and over pasture lands 4.3 °C higher compared to
646 the forest they replaced, caused by energy balance shifts. Ban-Weiss et al. (2011) and Davin
647 and de Noblet-Ducoudré (2010) added that in addition to the reduction of ET, the reduction of
648 surface roughness most likely enhanced the substantial local warming.

649

650 Also for non-Amazonian regions the replacement of forests by crops resulted in changes similar
651 to our observations. In temperate Argentina, Houspanossian et al. (2013) found that the
652 replacement of dry forests by crops resulted in an increase of albedo and still the forests
653 exhibited cooler canopies than croplands. The cooler canopies were a result of the higher



654 aerodynamic conductance that caused the capacity of tree canopies to dissipate heat into the
655 atmosphere and that both latent and sensible heat fluxes operate simultaneously cooling forest
656 canopies Houspanossian et al. (2013).

657

658 In a global analysis Li et al. (2015) showed that tropical forests generally have a low albedo,
659 but still the net energy gain caused by solar energy absorption is offset by a greater latent heat
660 loss via higher ET and that in the tropical forests the high ET cooling completely offsets the
661 albedo warming. For China, this cooling effect was also shown by Peng et al. (2014) who
662 compared LST, albedo and ET of plantation forests, grassland and cropland with forests.

663

664 For the USA, Weng et al. (2004) and for China, Yue et al. (2007) used NDVI as a vegetation
665 abundance indicator and also found areas with a high mean NDVI to have lower LST than areas
666 with a low mean NDVI, all suggesting that vegetation abundance is an important factor in
667 controlling the LST through higher ET rates. Our result support their assumptions by showing
668 the high correlation between NDVI – LST and ET – LST.

669

670 Our findings are also supported by modelling studies. Beltrán-Przekurat et al. (2012) found for
671 the Southern Amazon that conversion of wooded vegetation to soy bean plantations caused an
672 increase of the LST due to decreased latent heat and increased sensible heat fluxes. Climate
673 models also show the same warming trends and land surface modelling also project an increase
674 in surface temperatures following deforestation in the Brazilian Cerrado (Beltrán-Przekurat et
675 al., 2012; Loarie et al., 2011b). In a global analysis, Pongratz et al. (2006) showed the LST
676 increase of forest to cropland or pasture transitions, also driven by reduced roughness length,
677 increased aerodynamic resistance, and that the temperature response is intensified in forest to
678 clear land or bare land transitions (1.2 °C increase). Similar to observational studies, the



679 modelling results of Bathiany et al. (2010) show that ET is the main driver of temperature
680 changes in tropical land areas.

681

682 In understanding the effects of deforestation on biophysical variables in Indonesia, our study
683 identifies the following mechanisms: (a) reduction of ET decreases surface cooling, (b) reduced
684 surface roughness reduces air mixing in the surface layer and thus vertical heat fluxes, (c)
685 changes in albedo change the net radiation, (d) changes in energy partitioning in sensible and
686 latent heat and heat storage. The effect is an increase of the mean temperatures leading to
687 warming effects in all tropical climatic zones (Alkama and Cescatti, 2016). We point here that
688 our study (1) included a ground heat flux, but did not take into account the storage of heat in
689 the soil and the release of stored heat out of the soil during the daily cycle and (2) that the
690 Landsat satellite image was obtained under cloud free conditions with high shortwave radiation
691 input and low fraction of diffuse radiation. Therefore, the LST retrieved on cloud free days
692 might be overestimated compared cloudy days where the differences in LST between land uses
693 are supposed to be less when diffuse radiation increases.

694

695 Our study is the first to include the oil palm and rubber expansion in Indonesia. In Indonesia,
696 smallholders take 40% of the land under oil palm cultivation for their account (Dislich et al.,
697 2016). Since the landscape in the Jambi province is characterized by small-scale smallholder-
698 dominated mosaic including rubber and oil palm monocultures (Clough et al., 2016), studies
699 using medium to coarse resolution data are not able to capture the small scale changes and
700 processes at the small-scale level. By using high resolution Landsat data we were able to also
701 include the effects of land use change on biophysical variables and the underlying processes of
702 the small scale holder agriculture.

703



704 **4.4 Effects of land use change on the provincial surface temperature in the past decades**

705

706 The mean surface temperature of the Jambi province increased stronger during the morning
707 (10:30 am) and afternoon (1:30 pm) than during the evening (10:30 pm) and night (1:30 am).

708 Given that our results show a decrease of the NDVI in the same period, this suggests that the
709 observed increased trend of the day time province LST can be attributed to land cover changes

710 that occurred. Our assumption that the observed decreasing NDVI trend is caused by land
711 conversions is supported by two different studies which reported that in the Jambi province

712 between 2000 and 2011 (Drescher et al., 2016) and between 2000 and 2013 (Clough et al.,
713 2016) the forest area decreased and that the largest increases were for rubber, oil palm, and

714 agricultural and tree crop areas. The class ‘other land use types’ which includes urban areas
715 showed a minor increase (around 1%) which suggests that the decrease in NDVI was most

716 likely caused by forest cover loss and not by urban expansion (see Supporting information,
717 Table S9). The same observations on LULC change in Indonesia were also supported by Lee

718 et al. (2011), Margono et al. (2012, 2014), Paterson et al. (2015) and Luskin et al. (2014). Luskin
719 et al. (2014) showed that in the period 2000 – 2010 forests decreased by 17%, oil palm and

720 rubber area increased by 85% and 19%, respectively, in the Jambi province.

721

722 Given these trends in LULC changes, the observed LST trends were most likely caused by
723 gradual decrease of forest cover loss at the expense of agriculture and croplands. Our

724 assumptions are supported by findings of Silvério et al. (2015), Costa et al. (2007), Oliveira et
725 al. (2013), Spracklen et al. (2012) and Salazar et al. (2015) which indicate that land use

726 transitions in deforested areas likely have a strong influence on regional climate. Alkama and
727 Cescatti's (2016) analysis show that biophysical effects of changes in forest cover can

728 substantially affect the local climate by altering the average temperature, which is consistent
729 with our observations and can be related to the observed land use change in the Jambi province.



730 As Indonesia has undergone high rates of forest cover loss from 2000 to 2012 (Margono et al.,
731 2014), these findings support our assumptions that the observed LST increase in the Jambi
732 province was most likely caused by the observed land use changes.

733

734 To separate the effect of global warming from land-use change induced warming, we
735 considered areas with permanent and large enough forests as reference where changes are
736 mainly due to global warming. We find that LST of forests show either no significant trends (at
737 1:30 pm, 10:30 pm, 1:30 am) or just a clearly smaller increase of 0.03 °C per year at 10:30 am.
738 The difference between the LST trend of the province and of the forest at 10:30 am was 0.04
739 °C per year, resulting in a Δ LST of 0.6 °C between the province and forest in the period 2000
740 and 2015. Using the warming effects we found between forest and other land cover types
741 (Δ LST, Fig. 4a) and the observed land cover changes by Clough et al. (2016), Drescher et al.
742 (2016) (Supporting Information S9, table S9.1 and S9.2) we estimated the contribution of all
743 land cover types (except forest) to the Δ LST of the province between 2000 and 2015 to be
744 0.51°C out of 0.6°C observed above, which also supports our assumption that the increase of
745 the province LST was by 85% driven by land cover changes (see Supporting Information 9,
746 Table S9.1 & S9.2: Land use change analysis), with clear cut areas having a large contribution
747 as they have the largest warming effect.

748

749 The observed small, but significant increase in LST of forests by 0.03 °C per year at 10:30 am
750 reflects a LST change independent to land cover changes as the forest remained unchanged over
751 that time period. Potential driver of that LST increase is the general global air temperature trend
752 due to changes in radiative forcing or border effects (advection from warmer land uses), which
753 is similar to the 1994 - 2014 time series analysis of Kayet et al. (2016) – who showed a LST
754 increase for all land cover types ranging from wasted land, agriculture land, open forest, dense
755 forest, water bodies, built up.



756

757 The observed trends of province air temperature (Fig. 5f) were significant, suggesting that a
758 general warming due to global and regional effects contributes to the observed warming at
759 province level during day and night time, but is smaller than the land cover change induced
760 effects (Supporting Information S9, Table S9.1 & S9.2) at provincial level (Fig. 5a and 5b).

761

762 In our long term analysis on the regional effects of land use change we observed an increase in
763 the mean LST and mean air temperature in the 2000 - 2015 period, concurrent to a decrease of
764 the NDVI. The warming observed from MODIS LST data and from the air temperature
765 obtained from the independent ERA Interim Reanalysis in the Jambi province are most likely
766 caused by the observed decrease of the forest area and an increase oil palm, rubber and other
767 cash crop areas in the same period, with other effects such as radiative forcing changes and
768 additional natural effects playing a smaller role. Given the plan of the Indonesian governmental
769 to substantially expand oil palm productivity with an projected additional demand of 1 to 28
770 Mha in 2020 (Wicke et al., 2011), the strong warming effect we show for Jambi province may
771 serve as an indication of future changes in LST for other regions of Indonesia that will undergo
772 land transformations towards oil palm plantations.

773 The observed effects of land use change on the biophysical variables may have implications for
774 ecosystem services in the Jambi province beyond a pure warming effect. The high precipitation
775 in this region in combination with the reduced vegetation cover of bare land and young oil palm
776 plantations impose risks of soil erosion caused by surface run off. Less water infiltrates in the
777 soil, thereby decreasing the soil water storage that may lead to low water availability in the dry
778 season (Dislich et al., 2016; Merten et al., 2016). High surface temperatures in combination
779 with low water availability may make the vegetation and the surroundings more vulnerable for
780 fires.

781



782 **5 Conclusion**

783

784 In summary, we showed the importance of forests in regulating the local and regional climate.

785 We derived biophysical variables from satellite data, analyzed the biophysical impacts of

786 deforestation and on a local scale we found a general warming effect after forests are

787 transformed to cash or tree croplands (oil palm, rubber, acacia) in the Jambi province of

788 Sumatra. The warming effect after forest conversion results from the reduced evaporative

789 cooling, which was identified as the main determinant of regulating the surface temperature.

790 On a regional scale, we saw that the effects of land cover changes are reflected back in changes

791 of the LST, NDVI and air temperature of the Jambi province. The warming effect induced by

792 land cover change clearly exceeded the global warming effect. Understanding the effects of

793 land cover change on the biophysical variables may support policies regarding conservation of

794 the existing forests, planning and expansion of the oil palm plantations and possible

795 afforestation measures.

796

797



843 *Author contributions.* Clifton R. Sabajo conducted the research, fieldwork an analysis and
844 prepared the manuscript, which was reviewed by Gueric le Maire, Tania June, Ana Mejjide,
845 Olivier Rouspard and Alexander Knohl. Ana Mejjide and Alexander Knohl provided the
846 meteorological data.

Competing interests. The authors declare that they have no conflict of interest.

847 *Acknowledgements.* This research was funded by the Erasmus Mundus Joint Doctorate
848 Programme Forest and Nature for Society (EMJD FONASO) and the German Research
849 Foundation (DFG) through the CRC 990 “EForTS, Ecological and Socioeconomic Functions
850 of Tropical Lowland Rainforest Transformation Systems (Sumatra, Indonesia)” (subproject
851 A03). A special thanks to Huta Julu Bagus Putra, a.k.a. Monang, for his assistance and
852 translation during the field work in Indonesia. The authors state to have no conflict of interest.

853

854

855 **References**

856

857 Alkama, R. and Cescatti, A.: Biophysical climate impacts of recent changes in global forest
 858 cover, *Science*, 351(6273), 600–604, doi:10.1126/science.aac8083, 2016.

859 Ban-Weiss, G. A., Bala, G., Cao, L., Pongratz, J. and Caldeira, K.: Climate forcing and response
 860 to idealized changes in surface latent and sensible heat, *Environ. Res. Lett.*, 6(3), 34032, 2011.

861 Barsi, J. A., Barker, J. L. and Schott, J. R.: An Atmospheric Correction Parameter Calculator
 862 for a Single Thermal Band Earth-Sensing Instrument, *Geosci. Remote Sens. Symp. 2003*
 863 *IGARSS 03 Proc. 2003 IEEE Int.*, 5, 3014–3016 vol.5, doi:10.1109/IGARSS.2003.1294665,
 864 2003.

865 Barsi, J. A., Schott, J. R., Palluconi, F. D. and Hook, S. J.: Validation of a web-based
 866 atmospheric correction tool for single thermal band instruments, in *Proc. SPIE, Earth Observing*
 867 *Systems X*, vol. 5882, San Diego, California, USA., 2005.

868 Bastiaanssen, W. G. .: SEBAL-based sensible and latent heat fluxes in the irrigated Gediz
 869 Basin, Turkey, *J. Hydrol.*, 229(1–2), 87–100, doi:10.1016/S0022-1694(99)00202-4, 2000.

870 Bastiaanssen, W. G. M., Menenti, M., Feddes, R. A. and Holtslag, A. A. M.: A remote sensing
 871 surface energy balance algorithm for land (SEBAL) - 1. Formulation, *J. Hydrol.*, 212(1–4),
 872 198–212, doi:10.1016/s0022-1694(98)00253-4, 1998a.

873 Bastiaanssen, W. G. M., Pelgrum, H., Wang, J., Ma, Y., Moreno, J. F., Roerink, G. J. and van
 874 der Wal, T.: A remote sensing surface energy balance algorithm for land (SEBAL): Part 2:
 875 Validation, *J. Hydrol.*, 212–213, 213–229, doi:10.1016/S0022-1694(98)00254-6, 1998b.

876 Bathiany, S., Claussen, M., Brovkin, V., Raddatz, T. and Gayler, V.: Combined biogeophysical
 877 and biogeochemical effects of large-scale forest cover changes in the MPI earth system model,
 878 *Biogeosciences*, 7(5), 1383–1399, doi:10.5194/bg-7-1383-2010, 2010.

879 Beltrán-Przekurat, A., Pielke Sr, R. A., Eastman, J. L. and Coughenour, M. B.: Modelling the
 880 effects of land-use/land-cover changes on the near-surface atmosphere in southern South
 881 America, *Int. J. Climatol.*, 32(8), 1206–1225, doi:10.1002/joc.2346, 2012.

882 Bindhu, V. M., Narasimhan, B. and Sudheer, K. P.: Development and verification of a non-
 883 linear disaggregation method (NL-DisTrad) to downscale MODIS land surface temperature to
 884 the spatial scale of Landsat thermal data to estimate evapotranspiration, *Remote Sens. Environ.*,
 885 135, 118–129, doi:10.1016/j.rse.2013.03.023, 2013.

886 Boisier, J. P., de Noblet-Ducoudré, N. and Ciais, P.: Historical land-use-induced
 887 evapotranspiration changes estimated from present-day observations and reconstructed land-
 888 cover maps, *Hydrol. Earth Syst. Sci.*, 18(9), 3571–3590, doi:10.5194/hess-18-3571-2014, 2014.

889 Bridhikitti, A. and Overcamp, T. J.: Estimation of Southeast Asian rice paddy areas with
 890 different ecosystems from moderate-resolution satellite imagery, *Agric. Ecosyst. Environ.*,
 891 146(1), 113–120, doi:10.1016/j.agee.2011.10.016, 2012.

892 Bright, R. M., Zhao, K., Jackson, R. B. and Cherubini, F.: Quantifying surface albedo and other
 893 direct biogeophysical climate forcings of forestry activities, *Glob. Change Biol.*, 21(9), 3246–
 894 3266, doi:10.1111/gcb.12951, 2015.



- 895 Clough, Y., Krishna, V. V., Corre, M. D., Darras, K., Denmead, L. H., Meijide, A., Moser, S.,
 896 Musshoff, O., Steinebach, S., Veldkamp, E., Allen, K., Barnes, A. D., Breidenbach, N., Brose,
 897 U., Buchori, D., Daniel, R., Finkeldey, R., Harahap, I., Hertel, D., Holtkamp, A. M., Hörandl,
 898 E., Irawan, B., Jaya, I. N. S., Jochum, M., Klarner, B., Knohl, A., Kotowska, M. M.,
 899 Krashevskaya, V., Kreft, H., Kurniawan, S., Leuschner, C., Maraun, M., Melati, D. N.,
 900 Opfermann, N., Pérez-Cruzado, C., Prabowo, W. E., Rembold, K., Rizali, A., Rubiana, R.,
 901 Schneider, D., Tjitrosoedirdjo, S. S., Tjoa, A., Tschardtke, T. and Scheu, S.: Land-use choices
 902 follow profitability at the expense of ecological functions in Indonesian smallholder landscapes,
 903 *Nat. Commun.*, 7, 13137, 2016.
- 904 Coll, C., Wan, Z. and Galve, J. M.: Temperature-based and radiance-based validations of the
 905 V5 MODIS land surface temperature product, *J. Geophys. Res.*, 114(D20), 2009.
- 906 Coll, C., Galve, J. M., Sanchez, J. M. and Caselles, V.: Validation of Landsat-7/ETM+ Thermal-
 907 Band Calibration and Atmospheric Correction With Ground-Based Measurements, *Geosci.*
 908 *Remote Sens. IEEE Trans. On*, 48(1), 547–555, doi:10.1109/TGRS.2009.2024934, 2010.
- 909 Costa, M. H., Yanagi, S. N. M., Souza, P. J. O. P., Ribeiro, A. and Rocha, E. J. P.: Climate
 910 change in Amazonia caused by soybean cropland expansion, as compared to caused by
 911 pastureland expansion, *Geophys. Res. Lett.*, 34(7), doi:10.1029/2007GL029271, 2007.
- 912 Davin, E. L. and de Noblet-Ducoudré, N.: Climatic Impact of Global-Scale Deforestation:
 913 Radiative versus Nonradiative Processes, *J. Clim.*, 23(1), 97–112,
 914 doi:10.1175/2009JCLI3102.1, 2010.
- 915 Dee, D. P., Uppala, S. M., Simmons, A. J., Berrisford, P., Poli, P., Kobayashi, S., Andrae, U.,
 916 Balmaseda, M. A., Balsamo, G., Bauer, P., Bechtold, P., Beljaars, A. C. M., van de Berg, L.,
 917 Bidlot, J., Bormann, N., Delsol, C., Dragani, R., Fuentes, M., Geer, A. J., Haimberger, L.,
 918 Healy, S. B., Hersbach, H., Hólm, E. V., Isaksen, I., Kållberg, P., Köhler, M., Matricardi, M.,
 919 McNally, A. P., Monge-Sanz, B. M., Morcrette, J.-J., Park, B.-K., Peubey, C., de Rosnay, P.,
 920 Tavolato, C., Thépaut, J.-N. and Vitart, F.: The ERA-Interim reanalysis: configuration and
 921 performance of the data assimilation system, *Q. J. R. Meteorol. Soc.*, 137(656), 553–597,
 922 doi:10.1002/qj.828, 2011.
- 923 Dislich, C., Keyel, A. C., Salecker, J., Kisel, Y., Meyer, K. M., Auliya, M., Barnes, A. D.,
 924 Corre, M. D., Darras, K., Faust, H., Hess, B., Klasen, S., Knohl, A., Kreft, H., Meijide, A.,
 925 Nurdiansyah, F., Otten, F., Pe'er, G., Steinebach, S., Tarigan, S., Tölle, M. H., Tschardtke, T.
 926 and Wiegand, K.: A review of the ecosystem functions in oil palm plantations, using forests as
 927 a reference system, *Biol. Rev.*, doi:10.1111/brv.12295, 2016.
- 928 Drescher, J., Rembold, K., Allen, K., Beckschäfer, P., Buchori, D., Clough, Y., Faust, H., Fauzi,
 929 A. M., Gunawan, D., Hertel, D., Irawan, B., Jaya, I. N. S., Klarner, B., Kleinn, C., Knohl, A.,
 930 Kotowska, M. M., Krashevskaya, V., Krishna, V., Leuschner, C., Lorenz, W., Meijide, A., Melati,
 931 D., Nomura, M., Pérez-Cruzado, C., Qaim, M., Siregar, I. Z., Steinebach, S., Tjoa, A.,
 932 Tschardtke, T., Wick, B., Wiegand, K., Kreft, H. and Scheu, S.: Ecological and socio-economic
 933 functions across tropical land use systems after rainforest conversion, *Philos. Trans. R. Soc.*
 934 *Lond. B Biol. Sci.*, 371(1694), doi:10.1098/rstb.2015.0275, 2016.
- 935 Fall, S., Niyogi, D., Gluhovsky, A., Pielke, R. A., Kalnay, E. and Rochon, G.: Impacts of land
 936 use land cover on temperature trends over the continental United States: assessment using the
 937 North American Regional Reanalysis, *Int. J. Climatol.*, 30(13), 1980–1993,
 938 doi:10.1002/joc.1996, 2010.



- 939 Feddema, J. J., Oleson, K. W., Bonan, G. B., Mearns, L. O., Buja, L. E., Meehl, G. A. and
 940 Washington, W. M.: The Importance of Land-Cover Change in Simulating Future Climates,
 941 *Science*, 310(5754), 1674, doi:10.1126/science.1118160, 2005.
- 942 Hoffmann, W. A. and Jackson, R. B.: Vegetation–Climate Feedbacks in the Conversion of
 943 Tropical Savanna to Grassland, *J. Clim.*, 13(9), 1593–1602, doi:10.1175/1520-
 944 0442(2000)013<1593:VCFITC>2.0.CO;2, 2000.
- 945 Houspanossian, J., Nosetto, M. and Jobbágy, E. G.: Radiation budget changes with dry forest
 946 clearing in temperate Argentina, *Glob. Change Biol.*, 19(4), 1211–1222,
 947 doi:10.1111/gcb.12121, 2013.
- 948 Idso, S. B. and Jackson, R. D.: Thermal radiation from the atmosphere, *J. Geophys. Res.*,
 949 74(23), 5397–5403, doi:10.1029/JC074i023p05397, 1969.
- 950 Jiang, Y., Fu, P. and Weng, Q.: Assessing the Impacts of Urbanization-Associated Land
 951 Use/Cover Change on Land Surface Temperature and Surface Moisture: A Case Study in the
 952 Midwestern United States, *Remote Sens.*, 7(4), doi:10.3390/rs70404880, 2015.
- 953 Kayet, N., Pathak, K., Chakrabarty, A. and Sahoo, S.: Spatial impact of land use/land cover
 954 change on surface temperature distribution in Saranda Forest, Jharkhand, *Model. Earth Syst.*
 955 *Environ.*, 2(3), 1–10, doi:10.1007/s40808-016-0159-x, 2016.
- 956 Lawrence, D. and Vandecar, K.: Effects of tropical deforestation on climate and agriculture,
 957 *Nat. Clim. Change*, 5(1), 27–36, 2015.
- 958 Lee, X., Goulden, M. L., Hollinger, D. Y., Barr, A., Black, T. A., Bohrer, G., Bracho, R., Drake,
 959 B., Goldstein, A., Gu, L., Katul, G., Kolb, T., Law, B. E., Margolis, H., Meyers, T., Monson,
 960 R., Munger, W., Oren, R., Paw U, K. T., Richardson, A. D., Schmid, H. P., Staebler, R., Wofsy,
 961 S. and Zhao, L.: Observed increase in local cooling effect of deforestation at higher latitudes,
 962 *Nature*, 479(7373), 384–387, doi:10.1038/nature10588, 2011.
- 963 van Leeuwen, T. T., Frank, A. J., Jin, Y., Smyth, P., Goulden, M. L., van der Werf, G. R. and
 964 Randerson, J. T.: Optimal use of land surface temperature data to detect changes in tropical
 965 forest cover, *J. Geophys. Res. Biogeosciences*, 116(G2), doi:10.1029/2010JG001488, 2011.
- 966 Li, F., Jackson, T. J., Kustas, W. P., Schmugge, T. J., French, A. N., Cosh, M. H. and Bindlish,
 967 R.: Deriving land surface temperature from Landsat 5 and 7 during SMEX02/SMACEX, 2002
 968 *Soil Moisture Exp. SMEX02*, 92(4), 521–534, doi:10.1016/j.rse.2004.02.018, 2004.
- 969 Li, Y., Zhao, M., Motesharrei, S., Mu, Q., Kalnay, E. and Li, S.: Local cooling and warming
 970 effects of forests based on satellite observations, *Nat. Commun.*, 6 [online] Available from:
 971 <http://dx.doi.org/10.1038/ncomms7603>, 2015.
- 972 Liang, S.: Narrowband to broadband conversions of land surface albedo I: Algorithms, *Remote*
 973 *Sens. Environ.*, 76(2), 213–238, doi:10.1016/S0034-4257(00)00205-4, 2000.
- 974 Lim, Y.-K., Cai, M., Kalnay, E. and Zhou, L.: Observational evidence of sensitivity of surface
 975 climate changes to land types and urbanization, *Geophys. Res. Lett.*, 32(22),
 976 doi:10.1029/2005GL024267, 2005.
- 977 Lim, Y.-K., Cai, M., Kalnay, E. and Zhou, L.: Impact of Vegetation Types on Surface
 978 Temperature Change, *J. Appl. Meteorol. Climatol.*, 47(2), 411–424, 2008.



- 979 Loarie, S. R., Lobell, D. B., Asner, G. P., Mu, Q. and Field, C. B.: Direct impacts on local
980 climate of sugar-cane expansion in Brazil, *Nat. Clim. Change*, 1(2), 105–109,
981 doi:10.1038/nclimate1067, 2011a.
- 982 Loarie, S. R., Lobell, D. B., Asner, G. P. and Field, C. B.: Land-Cover and Surface Water
983 Change Drive Large Albedo Increases in South America, *Earth Interact.*, 15(7), 1–16, 2011b.
- 984 Longobardi, P., Montenegro, A., Beltrami, H. and Eby, M.: Deforestation Induced Climate
985 Change: Effects of Spatial Scale, *PLoS ONE*, 11(4), e0153357,
986 doi:10.1371/journal.pone.0153357, 2016.
- 987 Luskin, M. S., Christina, E. D., Kelley, L. C. and Potts, M. D.: Modern Hunting Practices and
988 Wild Meat Trade in the Oil Palm Plantation-Dominated Landscapes of Sumatra, Indonesia,
989 *Hum. Ecol.*, 42(1), 35–45, doi:10.1007/s10745-013-9606-8, 2014.
- 990 Mahmood, R., Pielke, R. A., Hubbard, K. G., Niyogi, D., Dirmeyer, P. A., McAlpine, C.,
991 Carleton, A. M., Hale, R., Gameda, S., Beltrán-Przekurat, A., Baker, B., McNider, R., Legates,
992 D. R., Shepherd, M., Du, J., Blanken, P. D., Frauenfeld, O. W., Nair, U. S. and Fall, S.: Land
993 cover changes and their biogeophysical effects on climate, *Int. J. Climatol.*, 34(4), 929–953,
994 doi:10.1002/joc.3736, 2014.
- 995 Margono, B. A., Turubanova, S., Zhuravleva, I., Potapov, P., Tyukavina, A., Baccini, A., Goetz,
996 S. and Hansen, M. C.: Mapping and monitoring deforestation and forest degradation in Sumatra
997 (Indonesia) using Landsat time series data sets from 1990 to 2010, *Environ. Res. Lett.*, 7(3),
998 34010, doi:10.1088/1748-9326/7/3/034010, 2012.
- 999 Margono, B. A., Potapov, P. V., Turubanova, S., Stolle, F. and Hansen, M. C.: Primary forest
1000 cover loss in Indonesia over 2000–2012, *Nat. Clim Change*, 4(8), 730–735, 2014.
- 1001 Marlier, M. E., DeFries, R., Pennington, D., Nelson, E., Ordway, E. M., Lewis, J., Koplitz, S.
1002 N. and Mickley, L. J.: Future fire emissions associated with projected land use change in
1003 Sumatra, *Glob. Change Biol.*, 21(1), 345–362, doi:10.1111/gcb.12691, 2015.
- 1004 Meijide, A., Röhl, A., Fan, Y., Herbst, M., Niu, F., Tiedemann, F., June, T., Rauf, A., Hölscher,
1005 D. and Knohl, A.: Controls of water and energy fluxes in oil palm plantations: Environmental
1006 variables and oil palm age, *Agric. For. Meteorol.*, 239, 71–85,
1007 doi:10.1016/j.agrformet.2017.02.034, 2017.
- 1008 Merten, J., Röhl, A., Guillaume, T., Meijide, A., Tarigan, S., Agusta, H., Dislich, C., Dittrich,
1009 C., Faust, H., Gunawan, D., Hein, J., Hendrayanto, Knohl, A., Kuzyakov, Y., Wiegand, K. and
1010 Hölscher, D.: Water scarcity and oil palm expansion: social views and environmental processes,
1011 *Ecol. Soc.*, 21(2), doi:10.5751/ES-08214-210205, 2016.
- 1012 Miettinen, J., Shi, C. and Liew, S. C.: Deforestation rates in insular Southeast Asia between
1013 2000 and 2010, *Glob. Change Biol.*, 17(7), 2261–2270, 2011.
- 1014 Miettinen, J., Hooijer, A., Wang, J., Shi, C. and Liew, S. C.: Peatland degradation and
1015 conversion sequences and interrelations in Sumatra, *Reg. Environ. Change*, 12(4), 729–737,
1016 doi:10.1007/s10113-012-0290-9, 2012.



- 1017 Mildrexler, D. J., Zhao, M. and Running, S. W.: A global comparison between station air
1018 temperatures and MODIS land surface temperatures reveals the cooling role of forests, *J.*
1019 *Geophys. Res. Biogeosciences*, 116(G3), doi:10.1029/2010JG001486, 2011.
- 1020 Nosetto, M. D., Jobbágy, E. G. and Paruelo, J. M.: Land-use change and water losses: the case
1021 of grassland afforestation across a soil textural gradient in central Argentina, *Glob. Change*
1022 *Biol.*, 11(7), 1101–1117, doi:10.1111/j.1365-2486.2005.00975.x, 2005.
- 1023 Oliveira, L. J. C., Costa, M. H., Soares-Filho, B. S. and Coe, M. T.: Large-scale expansion of
1024 agriculture in Amazonia may be a no-win scenario, *Environ. Res. Lett.*, 8(2), 24021, 2013.
- 1025 Paterson, R. R. M., Kumar, L., Taylor, S. and Lima, N.: Future climate effects on suitability for
1026 growth of oil palms in Malaysia and Indonesia, *Sci. Rep.*, 5, 14457, 2015.
- 1027 Peng, S.-S., Piao, S., Zeng, Z., Ciais, P., Zhou, L., Li, L. Z. X., Myneni, R. B., Yin, Y. and
1028 Zeng, H.: Afforestation in China cools local land surface temperature, *Proc. Natl. Acad. Sci.*,
1029 111(8), 2915–2919, 2014.
- 1030 Pongratz, J., Bounoua, L., DeFries, R. S., Morton, D. C., Anderson, L. O., Mauser, W. and
1031 Klink, C. A.: The Impact of Land Cover Change on Surface Energy and Water Balance in Mato
1032 Grosso, Brazil, *Earth Interact.*, 10(19), 1–17, 2006.
- 1033 Salazar, A., Baldi, G., Hirota, M., Syktus, J. and McAlpine, C.: Land use and land cover change
1034 impacts on the regional climate of non-Amazonian South America: A review, *Glob. Planet.*
1035 *Change*, 128, 103–119, doi:10.1016/j.gloplacha.2015.02.009, 2015.
- 1036 Salazar, A., Katzfey, J., Thatcher, M., Syktus, J., Wong, K. and McAlpine, C.: Deforestation
1037 changes land–atmosphere interactions across South American biomes, *Glob. Planet. Change*,
1038 139, 97–108, doi:10.1016/j.gloplacha.2016.01.004, 2016.
- 1039 Sheil, D., Casson, A., Meijaard, E., Van Noordwijk, M., Gaskell, J., Sunderland-Groves, J.,
1040 Wertz, K. and Kanninen, M.: The impacts and opportunities of oil palm in Southeast Asia: What
1041 do we know and what do we need to know?, Center for International Forestry Research
1042 (CIFOR), Bogor, Indonesia., 2009.
- 1043 Silvério, D. V., Brando, P. M., Macedo, M. N., Beck, P. S. A., Bustamante, M. and Coe, M. T.:
1044 Agricultural expansion dominates climate changes in southeastern Amazonia: the overlooked
1045 non-GHG forcing, *Environ. Res. Lett.*, 10(10), 104015, 2015.
- 1046 Snyder, W. C., Wan, Z., Zhang, Y. and Feng, Y.-Z.: Classification-based emissivity for land
1047 surface temperature measurement from space, *Int. J. Remote Sens.*, 19(14), 2753–2774,
1048 doi:10.1080/014311698214497, 1998.
- 1049 Sobrino, J. A., Jiménez-Muñoz, J. C. and Paolini, L.: Land surface temperature retrieval from
1050 LANDSAT TM 5, *Remote Sens. Environ.*, 90(4), 434–440, doi:10.1016/j.rse.2004.02.003,
1051 2004.
- 1052 Sobrino, J. A., Jiménez-Muñoz, J. C., Zarco-Tejada, P. J., Sepulcre-Cantó, G. and de Miguel,
1053 E.: Land surface temperature derived from airborne hyperspectral scanner thermal infrared data,
1054 *Remote Sens. Environ.*, 102(1–2), 99–115, doi:10.1016/j.rse.2006.02.001, 2006.
- 1055 Sobrino, J. A., Jimenez-Muoz, J. C., Soria, G., Romaguera, M., Guanter, L., Moreno, J., Plaza,
1056 A. and Martinez, P.: Land Surface Emissivity Retrieval From Different VNIR and TIR Sensors,



- 1057 Geosci. Remote Sens. IEEE Trans. On, 46(2), 316–327, doi:10.1109/TGRS.2007.904834,
1058 2008.
- 1059 Spracklen, D. V., Arnold, S. R. and Taylor, C. M.: Observations of increased tropical rainfall
1060 preceded by air passage over forests, *Nature*, 489(7415), 282–285, doi:10.1038/nature11390,
1061 2012.
- 1062 Verstraeten, W. W., Veroustraete, F. and Feyen, J.: Estimating evapotranspiration of European
1063 forests from NOAA-imagery at satellite overpass time: Towards an operational processing
1064 chain for integrated optical and thermal sensor data products, *Remote Sens. Environ.*, 96(2),
1065 256–276, doi:10.1016/j.rse.2005.03.004, 2005.
- 1066 Vlassova, L., Perez-Cabello, F., Nieto, H., Martín, P., Riaño, D. and de la Riva, J.: Assessment
1067 of Methods for Land Surface Temperature Retrieval from Landsat-5 TM Images Applicable to
1068 Multiscale Tree-Grass Ecosystem Modeling, *Remote Sens.*, 6(5), doi:10.3390/rs6054345,
1069 2014.
- 1070 Voogt, J. A. and Oke, T. R.: Effects of urban surface geometry on remotely-sensed surface
1071 temperature, *Int. J. Remote Sens.*, 19(5), 895–920, doi:10.1080/014311698215784, 1998.
- 1072 Wan, Z., Zhang, Y., Zhang, Q. and Li, Z.-L.: Quality assessment and validation of the MODIS
1073 global land surface temperature, *Int. J. Remote Sens.*, 25(1), 261–274,
1074 doi:10.1080/0143116031000116417, 2004.
- 1075 Weng, Q.: Thermal infrared remote sensing for urban climate and environmental studies:
1076 Methods, applications, and trends, *ISPRS J. Photogramm. Remote Sens.*, 64(4), 335–344,
1077 doi:10.1016/j.isprsjprs.2009.03.007, 2009.
- 1078 Weng, Q., Lu, D. and Schubring, J.: Estimation of land surface temperature–vegetation
1079 abundance relationship for urban heat island studies, *Remote Sens. Environ.*, 89(4), 467–483,
1080 doi:10.1016/j.rse.2003.11.005, 2004.
- 1081 Wicke, B., Sikkema, R., Dornburg, V. and Faaij, A.: Exploring land use changes and the role
1082 of palm oil production in Indonesia and Malaysia, *Land Use Policy*, 28(1), 193–206, 2011.
- 1083 Wukelic, G. E., Gibbons, D. E., Martucci, L. M. and Foote, H. P.: Radiometric calibration of
1084 Landsat Thematic Mapper thermal band, *Remote Sens. Environ.*, 28(0), 339–347,
1085 doi:10.1016/0034-4257(89)90125-9, 1989.
- 1086 Yue, W., Xu, J., Tan, W. and Xu, L.: The relationship between land surface temperature and
1087 NDVI with remote sensing: application to Shanghai Landsat 7 ETM+ data, *Int. J. Remote Sens.*,
1088 28(15), 3205–3226, doi:10.1080/01431160500306906, 2007.
- 1089 Zhang, Z. and He, G.: Generation of Landsat surface temperature product for China, 2000–
1090 2010, *Int. J. Remote Sens.*, 34(20), 7369–7375, doi:10.1080/01431161.2013.820368, 2013.
- 1091 Zhou, X. and Wang, Y.-C.: Dynamics of Land Surface Temperature in Response to Land-
1092 Use/Cover Change, *Geogr. Res.*, 49(1), 23–36, doi:10.1111/j.1745-5871.2010.00686.x, 2011.
- 1093
- 1094